Journal of Molecular Liquids 279 (2019) 640–648

Contents lists available at ScienceDirect

Journal of Molecular Liquids

journal homepage: www.elsevier.com/locate/molliq

Interaction of Congo Red, Evans Blue and Titan Yellow with doxorubicin in aqueous solutions. A molecular dynamics study

Anna Jagusiak [a], Tomasz Pańczyk [b,*]

[a] Chair of Medical Biochemistry, Faculty of Medicine, Jagiellonian University Medical College, ul. Kopernika 7, 31034 Cracow, Poland
[b] Institute of Catalysis and Surface Chemistry, Polish Academy of Sciences, ul. Niezapominajek 8, 30239 Cracow, Poland

ARTICLE INFO

Article history:
Received 5 December 2018
Received in revised form 25 January 2019
Accepted 3 February 2019
Available online 5 February 2019

Keywords:
Aggregation
Congo Red
Doxorubicin
Evans Blue
Titan Yellow
Molecular dynamics

ABSTRACT

Congo Red, Evans Blue and Titan Yellow were studied in pure component solutions and in mixtures with doxorubicin. Congo Red was analyzed in both unprotonated and protonated forms which mimics the neutral and acidic pH of solutions. The analysis was based on the molecular dynamics simulations with the second generation of the general amber force field, gaff2. The calculations results led to the conclusion that in pure component solutions the dyes and also doxorubicin exist in forms of single molecules or a few molecule aggregates. The exception is the protonated CR which forms large all-molecule aggregate. However, in the case of mixtures of dyes with doxorubicin we observed formation of larger aggregates consisting of dyes and doxorubicin molecules and accompanied by a few molecule clusters or just single molecules of the remaining dyes molecules. Within the aggregates the dyes molecules reveal a tendency to parallel alignment with, however, diverse intensities. The strongest tendency to formation of ribbon-like structures revealed Evans Blue and the ordering was the longest range in the case of Evans Blue. Other dyes revealed only short-range parallel alignment with the exception of the protonated Congo Red for which the formation of ribbon-like structures was strong. Among studied systems the strongest binding of doxorubicin was found in the case of the unprotonated Congo Red while the weakest – for the protonated Congo Red. Binding free energy of doxorubicin to the aggregates formed by other dyes was generally significant and the spontaneous detachment of doxorubicin from those aggregates was found as rather unlikely at normal conditions. This effect can be utilized in targeted delivery of this drug to immune complexes where it can be released from the aggregates.

1. Introduction

Azo and bis-azo dyes are extensively studied due to their widespread application in industry to colour various materials or as probe molecules in diverse chemical/biochemical research methodologies. For instance, Congo Red (CR) is often used as model dye molecule to study materials for removal of toxic compounds from water or wastewater [1–3]. However, CR reveals another important property that is a strong self-assembly tendency [4,5] and particularly its ability to react/interact specifically with amyloid proteins [6–8]. Evans Blue (EB) is known from its high affinity to serum albumin [9], moreover EB is often used in biochemistry to assess the permeability of the blood–brain barrier to macromolecules [10–12]. Titan Yellow TY was often used in colorimetric determination of magnesium ions [13,14] as well as in other analytical chemistry methods [15].

Many dyes molecules are able to change electronic density distribution or just overall molecular charge as a function of pH. Therefore, some of their properties like strength of intermolecular interactions or adsorption alter strongly and this can be utilized in construction of e.g. stimuli responsive drugs carriers. Indeed, in recent publications Panczyk et al. [16,17] proposed a concept of pH controlled carrier of doxorubicin DX in which the drug together with some dyes are encapsulated in the inner space of a carbon nanotube. The key factor was application of dyes with pK_a values close to 6, so the change of the protonation state of dyes led to co-release of DX from the carbon nanotube. CR was also studied in the context of drug delivery because it was found that the interaction of CR with carbon nanotubes was significantly modified upon pH change [18].

Congo Red, Evans Blue and Titan Yellow are also interesting because of their specific interaction with DX and some proteins. Their interaction with the albumin and light chain of antibodies was described, but also with native antibodies which form antigen - antibody complexes. In the case of interaction with antibodies, this is particularly important because these compounds interact only with immune complexes and do not interact with free antibodies [19–21]. This creates the possibility of targeted delivering of drugs associated with the ribbon like supramolecular structure of CR, selectively bound only to antibodies involved in the complex with the antigen.

* Corresponding author.
E-mail address: panczyk@vega.umcs.lublin.pl (T. Pańczyk).

https://doi.org/10.1016/j.molliq.2019.02.012

To our best knowledge interaction of doxorubicin with CR, EB and TY has not been carried out so far using molecular dynamics simulations. That methodology offers a deep, molecular level insight into the mechanism of interactions, energetics, thermodynamics or simply visual observation of the molecular structures. Therefore, this contribution provides new physical insights into processes occurring in mixtures of these dyes with doxorubicin or pure dyes solutions. This knowledge allows us to predict how the dyes can affect (or not) the state of the DX molecules when they interact with the specialized proteins.

2. Methods

All calculations were performed using the open source lammps code [22] and generation of input files for lammps was done using self-designed scripts. These scripts converted outputs from AcPype [23] python script into lammps input files. The AcPype utilizes various programms from AmberTools package [24] and generates complete force fields, including second generation of general amber force filed, (gaff2) in various formats. The partial charges of atoms need then to be determined according to resp. (restrained electrostatic potential) scheme [25] and this was done by utilizing RED server service [26]. Complete force field parameters for all molecules studied here are provided as supplementary information.

Water molecules were accounted for explicitly using the TIP3P water model as it is fully compatible with the amber family of force fields. The number of water molecules was ca. 17,000 depending on a system composition. Water molecules were kept rigid using the shake algorithm. Na^+ and Cl^- ions were added to the simulation box in the amounts accounting for the assumed ionic strength 0.145 mol L^{-1} and to neutralize total charge (see Table 1). The cutoff distance for both van der Waals and electrostatic interactions was 12 Å. Summation of the electrostatic interactions was carried out using the particle-particle particle-mesh [27] summation methodology. The calculations were carried out with the timestep 2 fs. The initial box size was 70 × 70 × 130 Å and the total number of atoms in each system was ca. 54,000. The calculation were carried out at constant pressure, constant temperature and constant number of atoms ensemble (npt) using the Noose-Hoover barostat. The calculations were carried out using own computational cluster build from scratch. A single job was normally run on 20 Pentium Xeon cores and efficiency was ca. 1.0–1.5 ns per day depending on the system composition.

The systems were first heated up from 310 K to 500 K at constant volume conditions and kept at 500 K for 1 ns. Next, the systems were cooled down to 310 K for 1 ns and equilibrated for the next 1 ns at constant temperature and constant pressure 1 atm conditions. Finally, the production runs were performed; they took at least 6 ns for each system studied. Moreover, each system was also subjected to biased simulations for the extra 2–4 ns and no significant changes were observed in that prolonged part of the calculations.

Table 1
Definitions of the analyzed systems. DX – doxorubicin, CRn – unprotonated Congo Red, CRp – protonted Congo Red, EB – Evans Blue, TY – Titan Yellow.

System	Formula/components	Number of molecules/ions		
		DX	DYE	Na^+, Cl^-, H_2O
DX	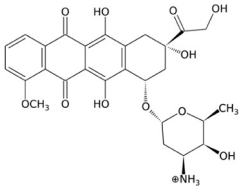	15	0	56, 71, 18,484
CRn	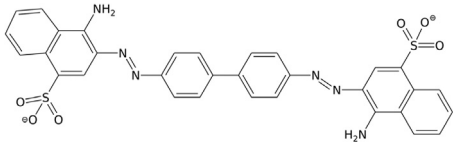	0	30	116, 56, 17,501
CRp	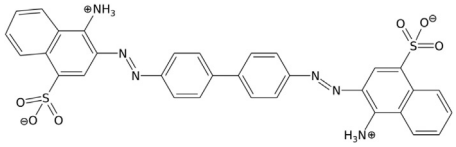	0	30	56, 56, 17,691
EB	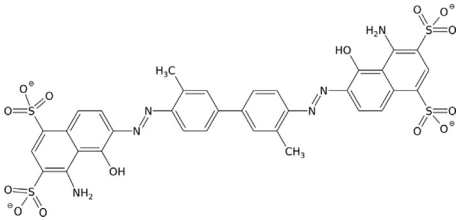	0	30	176, 56, 16,981
TY	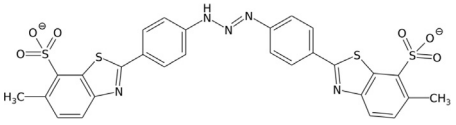	0	30	116, 56, 17,494
CRnDX	CRn + DX	15	30	116, 71, 16,800
CRpDX	CRp + DX	15	30	56, 71, 16,975
EBDX	EB + DX	15	30	176, 71, 16,272
TYDX	TY + DX	15	30	116, 71, 16,746

3. Results and discussion

3.1. Definition of the analyzed systems

The calculations involved 3 various dyes molecules among which Congo Red could be in its protonated or unprotonated form. Each dye was mixed (or not) with doxorubicin thus we finally assembled 9 independent systems, as defined in Table 1. All bis-azo dyes were initially in their *trans* forms as this form was found as the dominating one [28], however, the transitions to *cis* forms are rather easy and we should expect both forms with roughly the same populations at thermal equilibrium. Complete force field parameters and initial topologies of all molecules from Table 1 are provided as the supplementary electronic material. We chose gromacs files

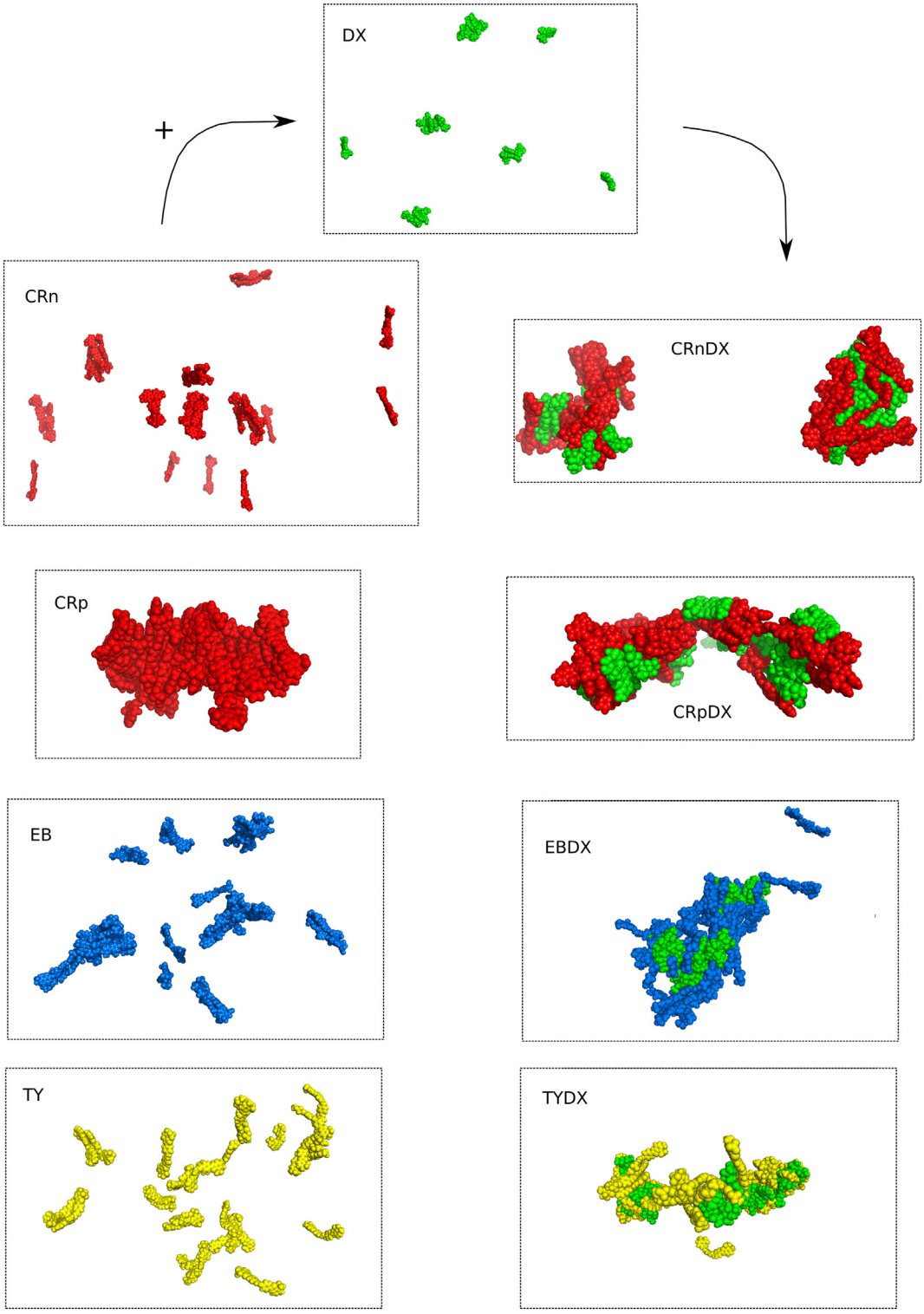

Fig. 1. Simulation snapshots of the studied systems before and after mixing the dyes with doxorubicin. The snapshots taken after 6 ns of calculation at constant temperature 310 K and constant pressure 1 atm and in 0.145 mol L^{-1} NaCl solution.

format for representation of the force field because it is relatively easy to phrase and widely used [29].

As mentioned, the calculations were carried out for quite a long time 6 ns and it was enough to draw reliable though still qualitative conclusions concerning the long-term behavior of the systems. We found that the state of each system is mainly dependent on the presence of doxorubicin, DX. The systems without DX, or with DX only, prefer molecularly dispersed states (or with only small aggregates). In turn, addition of DOX leads to formation of larger aggregates. Fig. 1 shows representative snapshots of the simulation boxes for all systems studied.

Initial distribution of molecules within the simulation box can formally determine their final configuration due to formation of transient states corresponding to local potential energy wells. Therefore, each configuration shown in Fig. 1 was obtained from similar initial distribution of molecules within the simulation box. DX and dyes were placed in well separated rows each containing 15 molecules.

Thus, the dyes formed two parallel rows and DX was added as the third and still parallel row containing 15 DX molecules. As a result, initial configurations represented totally separated subsets of DX and dyes molecules and the mixed states, shown in Fig. 1, appeared spontaneously during calculations. Of course, during preparation of the simulation boxes other initial arrangements of the molecules were produced and tested. However, we did not observe any effects related to those arrangements in longer runs and therefore we applied the above described approach for all the systems studied in production runs.

Development of the aggregates in the mixed dye + DX systems was found as quite a fast process. The aggregates started developing in early stages of the calculations (in the first 2 ns) i.e. during the heating stage the molecules already formed weakly bound pre-aggregates and they settled down to actually final forms during the cooling stage. Thus, during the equilibration stages and production runs the aggregates were already present though some exchange of molecules with the bulk occurred.

3.2. Aggregation of dyes and doxorubicin in solution

Looking at the simulation snapshots we can see that the protonated Congo Red differs significantly from the other dyes. It forms aggregates before mixing with DX. This was already observed in our previous work devoted to the analysis of CR with various protonation states and interacting with carbon nanotubes [18,30]. The protonated state of CR appears below pH 4–5 and therefore this is not a particularly interesting state of that molecule when its biochemical applications are considered. Moreover, at such low pH the conversion to the quinoid form of the protonated CR may occur [31]. The protonated CR forms, as seen, large aggregates and colloidal stability of such a solution must be weak. The other dyes, in turn, seem to form regular aqueous solutions as they exists as only small aggregates.

The division of molecules into aggregates of various sizes is very interesting phenomenon and deserves a closer analysis. Thus, Table 2 shows various pieces of information concerning the observed clustering and intermolecular interactions between various compounds. A classification of a given atom as belonging to a given aggregate is based on the distance criterion. Thus, a set of atoms, where each of it is within the cutoff distance 3.5 Å from one or more atoms within a fragment is a part of the same aggregate. Next, all such atoms are labeled by the same label and the number of distinct labels (aggregates) was computed.

Let us note that DX is not molecularly dispersed in the considered conditions of temperature and salt concentration. 15 DX molecules form 5–6 aggregates and the biggest one is composed of 4.4 (on average) DX molecules. There are also single molecules dispersed in solution as the smallest aggregate found in simulations is just a single DX molecule. The quantities max and min in Table 2 have quite simple meaning but in order to avoid any misunderstanding let us note that they were determined by searching for the biggest and the smallest aggregate in each simulation frame (snapshot) and averaging them over all simulation frames. Therefore, these quantities are not integer numbers and they do not sum to the total number of molecules because we skip aggregates which did not get the min or max flag.

Average aggregate size can be calculated by dividing the total number of molecules by the average number of aggregates. Thus, in the case of DX we get 2.5 which means that DX forms 2–3 molecule aggregates in solution. Obviously, this is only estimation of a static average aggregate size. In practice we observed dynamic changing of aggregates numbers, compositions and sizes. To sum up, DX is well soluble in the considered solvent and looking at the mean pair interaction energy between DX molecules we can conclude that this is due to electrostatic repulsion between charged DX ions. Of course, that repulsion is compensated to some extent by the interaction with water and salt ions and by dispersion interactions (which are always attractive). The presence of small a few molecule aggregates is possible due to such a compensation of the electrostatic repulsion because all these components are of similar order and are able to compensate each other depending on local orientation of molecules or density fluctuation.

In the case of neutral form of Congo Red, CRn, we also observed small aggregates well dispersed in the solvent. However, in this case the size of the largest aggregates reached 11.7 molecules that is almost half of the total amount of the CRn molecules. At the same time the mean number of aggregates is ca. 6.5 thus the rest of those 11.7 molecules is dispersed over ca. 5 other aggregates. The smallest aggregates are not bigger than 2 molecules. The general conclusion is that CRn forms many aggregates of various sizes however the biggest should not exceed 12 CRn molecules and such a cluster should still represent good colloidal stability. And, similarly like in the case of DX, the main source of good solubility is electrostatic repulsion between charged CRn molecules, as seen in E(Dye-Dye) large positive value.

Totally different behavior reveals CRp. In this case we observe a single aggregate containing all CRp molecules. Moreover, this aggregate is absolutely static as the standard deviation of the aggregate size is zero. Looking at pair energies we can see that CRp molecules attract each

Table 2
Values of various parameters of interest found in calculations. E(DX-DX) – mean pair interaction energy between DX molecules per single DX molecule; E(DX-Dye) – mean pair interaction energy between DX and dye molecules per single DX molecule E(Dye-Dye) – mean pair interaction energy between dye molecules per single dye molecule; N_{agg} - average number of aggregates; max – composition and size of an average biggest aggregate found in each simulation frame; min – composition and size of an average smallest aggregate found in each simulation frame.

	E(DX-DX), kJ mol^{-1}	E(DX-Dye), kJ mol^{-1}	E(Dye-Dye), kJ mol^{-1}	N_{agg}	Max	Min
DX	228.5 ± 8.0	0	0	5.89 ± 0.45	4.4 ± 1.2 DX	1.00 ± 0.03 DX
CRn	0	0	379.5 ± 43.2	6.41 ± 1.28	11.7 ± 2.6 CRn	1.5 ± 0.5 CRn
CRp	0	0	−543.8 ± 4.3	1.00 ± 0.00	30 ± 0 CRp	–
EB	0	0	902.2 ± 144.2	9.64 ± 1.83	11.07 ± 1.89 EB	1.00 ± 0.00 EB
TY	0	0	134.1 ± 21.1	7.31 ± 1.20	7.9 ± 1.17 TY	1.3 ± 0.67 TY
CRnDX	313.9 ± 8.6	−1223 ± 22	670.6 ± 27.8	2.00 ± 0.00	8 ± 0 DX, 15 ± 0 CRn	7 ± 0 DX, 15 ± 0 CRn
CRpDX	311.2 ± 21.9	−264.6 ± 9.1	−474.6 ± 4.9	1.00 ± 0.00	15 ± 0 DX, 30 ± CRp	–
EBDX	349.2 ± 2.5	−2208 ± 127	2502 ± 364	3.69 ± 1.21	15 ± 0 DX, 26.7 ± 0.9 EB	0 ± 0 DX, 1.3 ± 0.87 EB
TYDX	350.2 ± 13.1	−1362 ± 107	683.3 ± 61.5	2.97 ± 0.94	11.3 ± 3.49 DX, 20.8 ± 7.79TY	0 ± 0DX, 1.0 ± 0.03TY

other (negative energy) because the repulsive component coming from electrostatic interactions disappeared in this case. Thus, the protonated form of CR cannot form a stable aqueous solution and reduction of pH leads to precipitation of CR from solution as known from experimental observations.

Evans Blue and Titan Yellow behave similarly like unprotonated Congo Red. In both cases we observe ca. 10 and 7 aggregates with the standard deviation of 1.2 and 1.8. The largest aggregates are composed of roughly 11 and 8 molecules, respectively and they dynamically change the number of molecules by 1.2–1.8 molecule during the whole simulation time. The smallest aggregates are single molecules (EB) or 1–2 molecules (TY). The stabilization of solution is controlled by electrostatic repulsion and this effect is particularly strong in the case of EB as this molecule carries the highest charge −4e. TY is the smallest of the considered dyes and reveals the smallest E(Dye-Dye) energy though its charge is the same like CRn.

Considering mixtures of DX with dyes we can observe coalescence of both compounds into aggregates. In the case of neutral form of CR we can see 2 aggregates composed of mixture of DX with CRn, these aggregates are very stable as no fluctuations of the aggregates numbers or sizes are observed. As seen in Table 2, the largest and the smallest aggregates are roughly the same and differ only by one DX molecule. Moreover, there is no exchange of molecules between aggregates as all values of standard deviation are zero. It seems that the observed size of the aggregates, i.e. 15 CRn molecules plus 7–8 DX molecules, is thermodynamically the most probable and would be preserved in larger boxes, reaching macroscopic or even experimental sizes.

The analysis of pair interaction energies leads to the conclusion that the observed clustering is related to overcompensation of repulsion between identical compounds by attraction between mixed pairs of compounds. Obviously, the pair energies are dominated by the electrostatic components and remembering that CRn is charged negatively and DX positively, the understanding of the observed phenomena is easy and clear: the electrostatic stabilization of pure solutions is canceled after mixing. The same conclusion applies also to EBDX and TYDX systems.

The protonated CR after mixing with DOX gives structurally the same picture like pure CRp. We got a single and totally static aggregate containing all molecules present in the box. The pair energies show that addition of DX slightly reduced the dye-dye energy and the DX-dye is the smallest of analyzed cases. This might suggest that the strength of adsorption of DX in the CRp cluster is the smallest when compared to the other systems.

Concerning EBDX and TYDX systems we can conclude that mixing the pure compounds leads to formation of ca. 3–4 aggregates but with only one dominating in size. In the case of EBDX all DX resides in that large aggregate and the smallest aggregates are just single EB molecules. TYDX also reveals existence of one large aggregate in which most of DX is bound. However, large fluctuations of that aggregate composition mean that there exists quite intense mass exchange between that large aggregate and transient a few molecule aggregates in its neighborhood. The smallest aggregates do not contain DX at all. Some residual DX molecules probably belong to the mentioned transient aggregates.

3.3. Planarity and spatial arrangements of dyes molecules

Another important factor which deserves analysis in the case of bisazo dyes is the shape of a molecule. Normally, all the studied dyes molecules should be fairly flat and any deviation from the planar shape can be related to external forces acting on such a molecule. Due to the planar shape of molecules the dyes can form rod-like or ribbon-like supramolecular mesophases in water solutions [5] due to mechanism of face-to-face stacking, which is a well-known property of Congo Red, for instance [4,7,32,33].

Quantitative analysis of the “planarity” of a molecule involves construction of the best-fit plane in 3D which passes through the centers of atoms forming that molecule. Quantitative measure of the degree of planarity can be the residual sum of squares (RSS) from fitting the model plane to atomic coordinates. Such a fitting has been done for each molecule in each simulation frame by utilizing the scheme of the singular value decomposition (SVD) of atomic coordinates matrix. Not going into technical details, the output from the SVD gives all quantities of interest, i.e. the least singular value is the square root of the residual sum of squares while the corresponding eigenvector gives components of the vector which is orthogonal to that best-fit plane. Fig. 2 shows distribution of the quantity defined as:

$$\langle d \rangle = \frac{\sqrt{RSS}}{N} \tag{1}$$

where N is the number of atoms in the molecule. $\langle d \rangle$ physically means a mean distance of an atom from its projection into the best fit plane passing through the molecule. Because $\langle d \rangle$ is expressed as per atom quantity it can be compared between various molecules and its meaning is: the smaller $\langle d \rangle$ the more planar molecule is.

Fig. 2 shows the distribution of $\langle d \rangle$ which was determined by counting the molecules with the same $\langle d \rangle$ and determining the probability of observation of a given value of $\langle d \rangle$ in the whole simulation time. The bottom part of Fig. 2 visualizes the most important states of the molecules, i.e. the minimal value of $\langle d \rangle$ observed (highly planar case), the most probable state and the maximum value of $\langle d \rangle$ observed (least planar case). They correspond to the headings min, peak and max, respectively.

Analysis of Fig. 2 leads to several important conclusions. Namely, all the considered molecules preserve their planar shape, though with

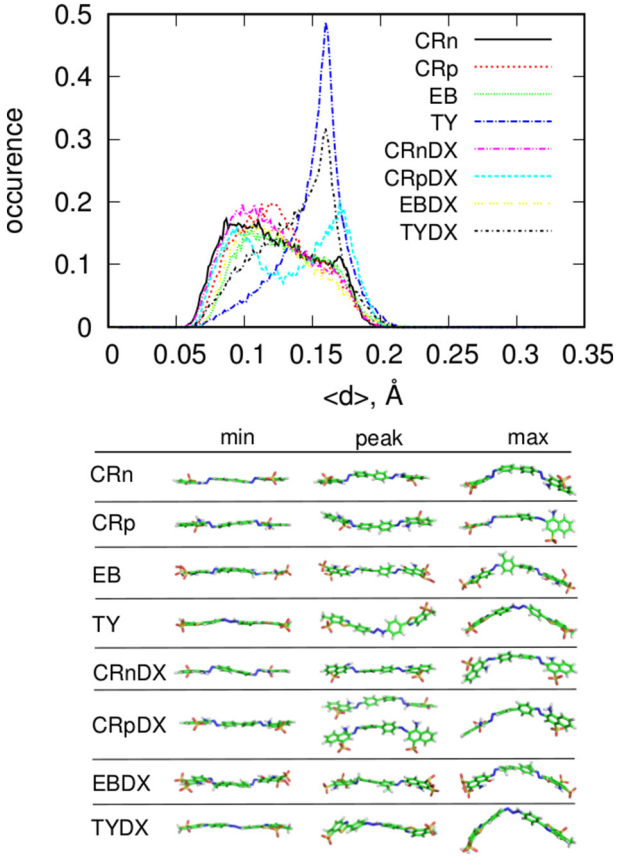

Fig. 2. The upper part shows distributions of the planarity parameter $\langle d \rangle$ of dyes molecules, defined in Eq. (1), for every studied system. The bottom part visualizes dyes molecules corresponding to the minimal and maximal value of $\langle d \rangle$ detected while the molecules in the “peak” column represent the most abundant states, that is with $\langle d \rangle$ corresponding to its maximum probability.

diverse quality, either in pure component or in a mixtures with DX. The visualizations of the most and the least planar cases give us a notion what happens in the middle but these particular shapes are rarely observed, in fact. Of course, the most likely states are the ones denoted as 'peak' and they correspond to the maximum value of the occurrence. But, as seen, most of the systems reveal rather uniform distribution of shapes with rather weakly pronounced maximum. The exception is TY and TYDX and also CRpDX where the shapes of the distributions differ significantly from the others. The CRpDX reveal two-modal distribution and these two different shapes of the CRp molecules are visualized in Fig. 2.

CRn and EB reveal very similar behavior and these molecules are actually the most planar as the peaks are shifted to the left when compared to TY and CRp. Also, formation of mixtures with DX only slightly affects the very good planarity of these molecules. This means that CRn and EB and also CRnDX and EBDX are able to form ribbon like structures as parallel alignment between molecules is easy to achieve and probably enhances intermolecular interactions. On the other hand, TY prefers states which are significantly bent though these molecules are able to reach highly planar structures. Moreover, TY reveals quite sharp peak which means that most of the molecules represent very similar and little planar structure. This peak becomes more diffuse after addition of DX, thus we can conclude that interaction with DX favors transition to more planar TY molecules. That structure of TY molecules might affect their ability of forming ribbon-like micelles with or without DX, however, it is difficult to draw more strict conclusions from this study. Interesting behavior reveals also CRpDX system where two peaks are observed. The protonated CR is less flat than its neutral counterpart as seen in Fig. 1 and addition of DX splits that structure into more and less planar ones with roughly the same populations.

The observed ability of keeping planar shapes of considered dyes molecules makes it possible to define an angle between any two molecules and further to detect creation of layered mesophases or just ribbons. From the SVD we got components of vectors orthogonal to the best-fit planes for each molecule. Thus, the normalized dot product of two vectors allows us to find the cosine of angle between the two vectors (molecules). Further, by measuring that angle for any given pair of molecules within the simulation frame and by summing over all frames allows us to determine the probability distribution of those angles for a given system. The method does not distinguish whether the molecules are close to each other or far away, simply all pairs of molecules are accounted for.

Fig. 3 shows the distribution of angles θ between any two dyes molecules determined according to the above scheme. The physical significance of these distributions is following: the higher value of the occurrence then the more likely is observation of the given angle and angles close to 0 or 180° represent parallel alignment of molecules. The fairly flat segments of the distributions in the range from 40 to 140° mean that no particular angle between molecules is preferred. However, in all the systems angles <40 and >140 are more likely than the reference state, i.e. 40–140°. This means that there is a preference towards parallel alignment though with diverse intensity.

The protonated form of Congo Red differs from the other cases either in pure component solution or in the mixture with DOX. Parallel orientation of molecules strongly dominates other alignments and this is related to formation of big aggregates in which the mutual orientation of molecules are almost intact. However, that stationary orientation is mainly parallel as seen in large values of the occurrence for 0 and 180°. The presence of DX destroys to some extent that ordering of CRp molecules though still the orientations close to parallel dominate strongly over other possible cases. Thus, the result shown in Fig. 3 supports a common statement that CR forms ribbon mesophases (micelles) in solution but this concern only the protonated form of CR. The neutral CR reveals only moderate occurrence of parallel molecules. They are only visible in pure component solution and therefore the enhanced probability of parallel orientations corresponds mainly to the closest neighbors alignment. The mixture of CRn with DX reveals rather small

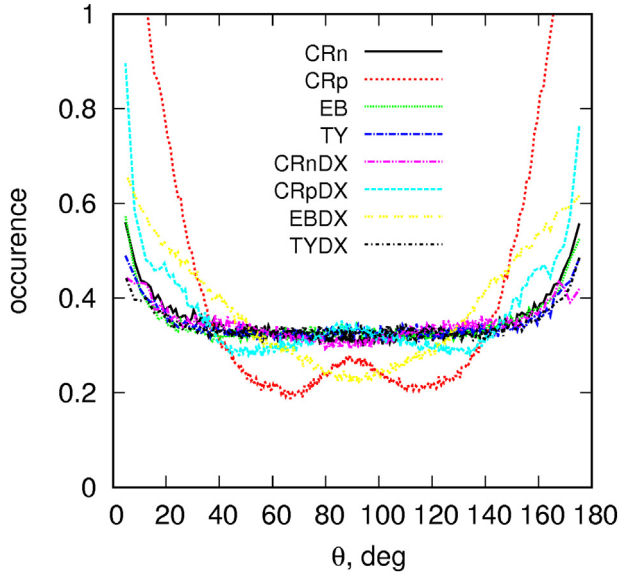

Fig. 3. Distribution of angles θ between any pair of dyes molecules determined for all simulation frames.

occurrence of parallel molecules. They are in a form of only two large aggregates and therefore the observed small occurrence of 0 and 180° means that CRn molecules are randomly distributed within the aggregates. Some small increase of the occurrence at terminal part of the distribution is related to short range ordering. Indeed, visual analysis of the aggregates structures (Fig. 4) leads to the conclusion that CRn forms 2–3 molecule stacks which are randomly oriented in reference to the other stacks and DX molecules fit into spaces between the stacks.

Generally, the above picture applies to the other dyes; parallel orientation is preserved to some small extent and must be attributed to the nearest neighbors alignment only. In pure component systems this is obvious because the molecules are in forms of small aggregates dispersed in solution. In the case of mixtures with DX the distributions are almost the same and thus we must conclude that the alignment must be similar, i.e. concerns only the nearest neighbors. However, EB differs from the above scheme. The pure component system indeed must be associated with the parallel alignment of the nearest neighbors but the mixture with DOX reveals enhanced occurrence of angles close to the parallel alignment and this must be attributed to the ordering at larger distances. Indeed, looking at Fig. 4 we can see that EBDX system reveals existence of long sandwiches EB mixed with DX and parallel alignment is preserved for both molecules at large distances.

3.4. Free energies of doxorubicin binding within the aggregates

Another interesting factor which needs attention is a binding energy of a DX molecule with an aggregate formed in solution. This factor informs about relative stabilities of dye-DX aggregates and can be used as an estimate of an aggregate lifetime in solution. The binding energies of a DX with the rest of an aggregate were determined as potentials of mean force during enforced detachment of that DX molecule from the aggregate. For that purpose we utilized the metadynamics biasing method [34]. This method adds gaussian hills to the system hamiltonian at a given position/value of the considered collective variable localized in a potential energy well and, as a result, the state of the system changes in such a way that it finally escapes from that energy well. During this process information about the parameters of the gaussian hills and their frequency is collected and can be used to recover the potential of mean force, pmf, associated with the escape from the potential energy well.

In this particular case the potential energy well is simply the state when the DX molecule is a part of the aggregate. The transfer of this

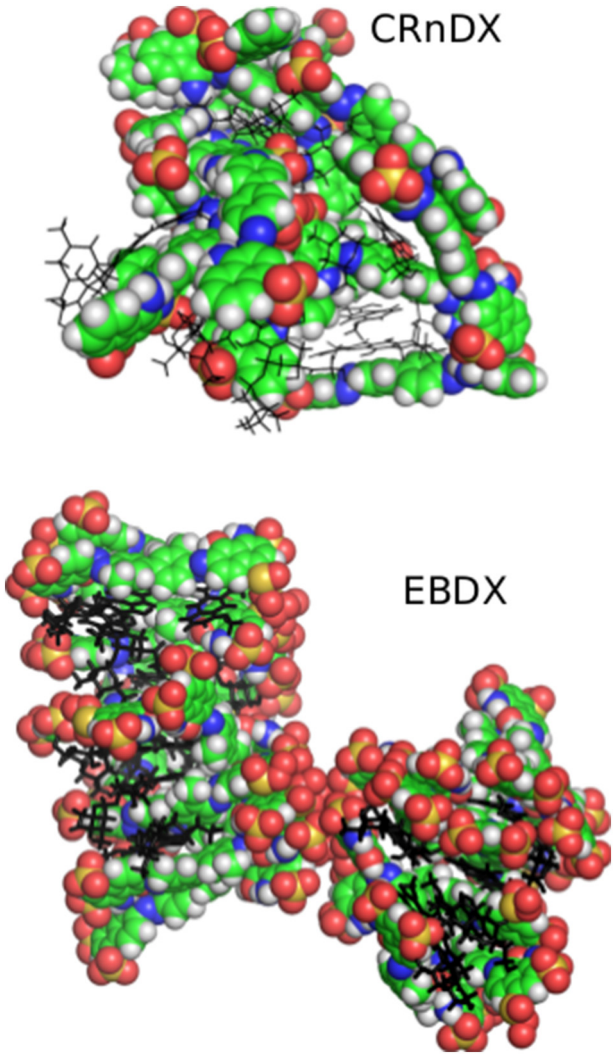

Fig. 4. Snapshots of the CRnDX and EBDX showing parallel orientation of dyes molecules. DX molecules are represented as black sticks for clarity of presentation.

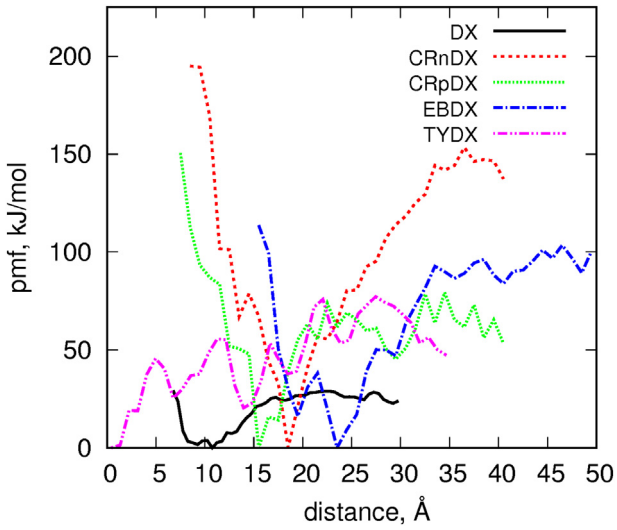

Fig. 5. Potentials of mean force, pmf, determined in metadynamics runs for all the systems containing DX. The gaussian hills had the heights of 0.5 kJ mol^{-1} and their widths (typically 0.5 Å) were related to the grid density. The insertion frequency was 2500 ns^{-1}.

molecule from the aggregate to the bulk is just the escape from the potential energy well. This escape is quantitatively measured as a distance between centers of masses of the DX molecule and the aggregate (collective variable). Fig. 5 shows the determined pmf's for all the systems where dye-DX aggregates were formed, for comparison, also the case of pure DX in solution is presented. The positions of the minimums differ strongly when going from system to system but this is related to somewhat arbitrary choice of the DX molecule to which the bias is added. The choice of the DX molecule affects to some extant also the depths of the pmfs but this should not lead to significant qualitative differences between the studied systems.

As seen in Fig. 1, doxorubicin forms small aggregates in the pure component solution. Thus, the pmf in Fig. 5 corresponds to the detachment process of a single DX molecule from the largest aggregate found, i.e. the one containing 3 DX molecules. The depth of the pmf minimum is just the free energy difference between the bound state (adsorption) and the desorbed state and informs about the thermodynamic stability of the adsorbed state. In the case of DX that value is 29 kJ mol^{-1} thus the aggregates are rather transient structures which form and decompose reversibly.

In the case of mixed systems there is always one large aggregate which is in equilibrium with a few smaller ones or just single dyes molecules. The exception is CR at the neutral pH where two almost identical aggregates were formed. Therefore, the detachment of the DX molecule from the largest aggregate was carried out in every case since it is the most natural choice. It is very likely that the largest aggregates are representative of the most likely aggregate in the limit of macroscopic system size. However, we cannot guarantee that the binding energy determined using these largest aggregates is the average value which could be found experimentally.

The strongest adsorption of DX is found in the CRnDX system. In this case the energy reaches 150 kJ mol^{-1} and we can conclude that DX is irreversibly attached to Congo Red aggregate and such a construct will be very difficult to destroy during interaction with other molecules (e.g. proteins). Most probably, DX will be deactivated when mixed with the neutral form of Congo Red in solution. Contrary to that, the protonated form of Congo Red reveals actually the weakest (among the studied dyes) affinity to DX. The free energy of DX adsorption on the CRp aggregate is 71 kJ mol^{-1}. This value means that spontaneous detachment of DX is rather unlikely, however, during interaction with other molecules the competing forces can prevail the interaction with the CRp. Interestingly, that small value of the free energy compares well with the smallest E(DX-Dye) value shown in Table 2. Though the CRp forms very large and stable aggregate the adsorption or incorporation of DX on/in its structure is not very strong. The recognized property of CR that is strong binding of DX at neutral pH and significant reduction of the binding energy at acidic pH can be utilized in realization of pH triggered release of DX at tumor sites. It is well known that tumors reveal reduced pH due to anaerobic glycolysis processes. However, this concept needs further studies using more relevant computational models.

Titan Yellow reveals actually the same value of binding free energy like CRp i.e. 76 kJ mol^{-1}. The lack of minimum in this case is due to the fact that centers of masses of both TY and the aggregate from which it detaches can overlap and this state corresponds to the energy minimum. That value can be considered as high and spontaneous desorption of DX is rather unlikely. But the presence of other molecules, particularly proteins can affect the state of DX molecules and they can be taken away from the aggregate when the affinity to protein will be high. Binding of DX to the EBDX aggregate is strong, the free energy difference is 97 kJ mol^{-1} and such an energy makes the adsorption irreversible. Interaction with other molecules can obviously be even stronger but generally doxorubicin seems to be locked strongly in the EBDX aggregates.

General conclusion concerning the binding energy of DX within the dyes aggregates is that DX is kept within the aggregates quite strongly and without a presence of other species the binding should be classified

as irreversible. The order of binding strengths is following (from the strongest to the weakest): CRn, EB, TY, CRp. However, this strong biding of DX to dyes aggregates can be potentially utilized in construction of the drug delivery vehicles. It is known that CR or other dyes aggregates form specific complexes with many proteins, including antibodies bound to the antigen and amyloids, in particular [19–21]. Interaction of the aggregate with the antibody may lead to the release of DX due to competitive many body interactions. However, such a mechanism needs further and dedicated studies.

4. Summary and conclusions

Molecular dynamics analysis of the behavior of Congo Red, Evans Blue and Titan Yellow dyes with or without doxorubicin in aqueous solution allowed us to draw several important conclusions concerning their properties. Namely, it was observed that all dyes (except of protonated CR) and also DX are molecularly dispersed or form aggregates in aqueous media. The sizes of these aggregates are rather small, including individual molecules, and the largest observed were not bigger than 12 molecules. Only in the case of protonated CR all dye molecules formed a single and big aggregate. Mixing of dyes with DX leads to formation of a few DX-dye aggregates which contain all DX molecules present in the solution. They are much bigger than in the case of pure dyes and contain from 15 to ca. 27 dye molecules. This behavior is associated with the compensation of the electrostatic charges of dyes (negative) by positively charged DX molecules. Within the aggregates we detected fairly well preserved parallel alignment of dye molecules but that ordering is observed mainly at short distances; only EB is able to preserve parallel alignment of molecules at relatively long distances. However, all dyes molecules prefer relatively flat conformations though formally they can exist in bent as well. Determination of the binding energy of DX within the aggregates led to conclusion that DX is quite strongly absorbed by dyes aggregates and spontaneous desorption is rather unlikely. This effect can be utilized in targeted delivery of this drug to immune complexes where it can be released from the aggregates. An interesting feature of CR is that the free energy of DX absorption in the aggregates is pH dependent; at neutral pH DX is strongly bound to the CRn while at acidic pH the binding is the weakest among the studied systems.

Acknowledgments

A. J. acknowledges financial support from the National Science Centre, Poland grant no. 2016/21/D/NZ1/02763; T. P. acknowledges financial support from the statutory research fund of ICSC PAS.

Appendix A. Supplementary data

Supplementary data to this article can be found online at https://doi.org/10.1016/j.molliq.2019.02.012.

References

[1] R. Saleh, A. Taufik, Degradation of methylene blue and congo-red dyes using fenton, photo-fenton, sono-fenton, and sonophoto-fenton methods in the presence of iron (II,III) oxide/zinc oxide/graphene (Fe_3O_4/ZnO/graphene) composites, Sep. Purif. Technol. 210 (2019) 563–573, https://doi.org/10.1016/j.seppur.2018.08.030.
[2] S.M. Prabhu, A. Khan, M. Hasmath Farzana, G.C. Hwang, W. Lee, G. Lee, Synthesis and characterization of graphene oxide-doped nano-hydroxyapatite and its adsorption performance of toxic diazo dyes from aqueous solution, J. Mol. Liq. 269 (2018) 746–754, https://doi.org/10.1016/j.molliq.2018.08.044.
[3] H. Zhang, H. Chen, S. Azat, Z.A. Mansurov, X. Liu, J. Wang, X. Su, R. Wu, Super adsorption capability of rhombic dodecahedral Ca-Al layered double oxides for Congo red removal, J. Alloys Compd. 768 (2018) 572–581, https://doi.org/10.1016/j.jallcom.2018.07.241.
[4] P. Spólnik, B. Stopa, B. Piekarska, A. Jagusiak, L. Konieczny, J. Rybarska, M. Król, I. Roterman, B. Urbanowicz, J. Zięba-Palus, The use of rigid, fibrillar Congo red nanostructures for scaffolding protein assemblies and inducing the formation of amyloid-like arrangement of molecules: use of rigid, fibrillar Congo red nanostructures, Chem. Biol. Drug Des. 70 (6) (2007) 491–501, https://doi.org/10.1111/j.1747-0285.2007.00589.x.
[5] M. Skowronek, B. Stopa, L. Konieczny, J. Rybarska, B. Piekarska, E. Szneler, G. Bakalarski, I. Roterman, Self-assembly of Congo red—a theoretical and experimental approach to identify its supramolecular organization in water and salt solutions, Biopolymers 46 (5) (1998) 267–281, https://doi.org/10.1002/(SICI)1097-0282(19981015)46:5<267::AID-BIP1>3.0.CO;2-N.
[6] B. Caughey, R.E. Race, Potent inhibition of scrapie-associated PrP accumulation by Congo red, J. Neurochem. 59 (2) (1992) 768–771.
[7] B. Stopa, A. Jagusiak, L. Konieczny, B. Piekarska, J. Rybarska, G. Zemanek, M. Król, P. Piwowar, I. Roterman, The use of supramolecular structures as protein ligands, J. Mol. Model. 19 (11) (2013) 4731–4740, https://doi.org/10.1007/s00894-012-1744-1.
[8] C. Reichhardt, L. Cegelski, The Congo red derivative FSB binds to curli amyloid fibers and specifically stains curliated E. coli, PLoS One 13 (8) (2018), e0203226. https://doi.org/10.1371/journal.pone.0203226.
[9] O. Jacobson, D.O. Kiesewetter, X. Chen, Albumin-binding Evans Blue derivatives for diagnostic imaging and production of long-acting therapeutics, Bioconjug. Chem. 27 (10) (2016) 2239–2247, https://doi.org/10.1021/acs.bioconjchem.6b00487.
[10] M. Kuriakose, K.V. Rama Rao, D. Younger, N. Chandra, Temporal and spatial effects of blast overpressure on blood-brain barrier permeability in traumatic brain injury, Sci. Rep. 8 (1) (2018)https://doi.org/10.1038/s41598-018-26813-7.
[11] M. Maloveska, J. Danko, E. Petrovova, L. Kresakova, K. Vdoviakova, A. Michalicova, A. Kovac, V. Cubinkova, D. Cizkova, Dynamics of Evans blue clearance from cerebrospinal fluid into meningeal lymphatic vessels and deep cervical lymph nodes, Neurol. Res. 40 (5) (2018) 372–380, https://doi.org/10.1080/01616412.2018.1446282.
[12] H. Alluri, M. Grimsley, C. Anasooya Shaji, K.P. Varghese, S.L. Zhang, C. Peddaboina, B. Robinson, M.R. Beeram, J.H. Huang, B. Tharakan, Attenuation of blood-brain barrier breakdown and hyperpermeability by calpain inhibition, J. Biol. Chem. 291 (53) (2016) 26958–26969, https://doi.org/10.1074/jbc.M116.735365.
[13] J. Ch. van Wesemael, The determination of magnesium with titan yellow, Anal. Chim. Acta 25 (3) (1961) 238–247, https://doi.org/10.1016/0003-2670(61)80153-0.
[14] M.C. Bowling, P.T. Wertlake, Selective staining of magnesium by titan yellow applied to incinerated tissue sections, Stain. Technol. 41 (6) (1966) 329–331, https://doi.org/10.3109/10520296609116334.
[15] X. Liu, Z. Zhang, J. Peng, Y. He, High-performance liquid chromatography with resonance Rayleigh scattering detection for determining four tetracycline antibiotics, Anal. Methods 6 (23) (2014) 9361–9366, https://doi.org/10.1039/C4AY01747A.
[16] T. Panczyk, P. Wolski, L. Lajtar, Coadsorption of doxorubicin and selected dyes on carbon nanotubes. Theoretical investigation of potential application as a PH-controlled drug delivery system, Langmuir 32 (19) (2016) 4719–4728, https://doi.org/10.1021/acs.langmuir.6b00296.
[17] P. Wolski, K. Nieszporek, T. Panczyk, Pegylated and folic acid functionalized carbon nanotubes as PH controlled carriers of doxorubicin. Molecular dynamics analysis of the stability and drug release mechanism, Phys. Chem. Chem. Phys. 19 (13) (2017) 9300–9312, https://doi.org/10.1039/C7CP00702G.
[18] T. Panczyk, P. Wolski, A. Jagusiak, M. Drach, Molecular dynamics study of Congo red interaction with carbon nanotubes, RSC Adv. 4 (88) (2014) 47304–47312, https://doi.org/10.1039/C4RA06806H.
[19] K. Chłopaś, A. Jagusiak, L. Konieczny, B. Piekarska, I. Roterman, J. Rybarska, B. Stopa, G. Zemanek, E. Bielańska, P. Piwowar, et al., The use of titan yellow dye as a metal ion binding marker for studies on the formation of specific complexes by supramolecular Congo red, Bio-Algorithms Med-Syst. 11 (1) (2015) 9–17, https://doi.org/10.1515/bams-2015-0001.
[20] B. Piekarska, A. Drozd, L. Konieczny, M. Król, W. Jurkowski, I. Roterman, P. Spólnik, B. Stopa, J. Rybarska, The indirect generation of long-distance structural changes in antibodies upon their binding to antigen, Chem. Biol. Drug Des. 68 (5) (2006) 276–283, https://doi.org/10.1111/j.1747-0285.2006.00448.x.
[21] I. Roterman-Konieczna, L. Konieczny (Eds.), Self-assembled Molecules - New Kind of Protein Ligands: Supramolecular Ligands, SpringerOpen, Cham, 2018.
[22] S. Plimpton, Fast parallel algorithms for short-range molecular dynamics, J. Comput. Phys. 117 (1) (1995) 1–19, https://doi.org/10.1006/jcph.1995.1039.
[23] A.W. Sousa da Silva, W.F. Vranken, ACPYPE - AnteChamber PYthon Parser InterfacE, BMC Res. Notes 5 (1) (2012) 367, https://doi.org/10.1186/1756-0500-5-367.
[24] D.A. Case, T.E. Cheatham, T. Darden, H. Gohlke, R. Luo, K.M. Merz, A. Onufriev, C. Simmerling, B. Wang, R.J. Woods, The amber biomolecular simulation programs, J. Comput. Chem. 26 (16) (2005) 1668–1688, https://doi.org/10.1002/jcc.20290.
[25] C.I. Bayly, P. Cieplak, W. Cornell, P.A. Kollman, A well-behaved electrostatic potential based method using charge restraints for deriving atomic charges: the RESP model, J. Phys. Chem. 97 (40) (1993) 10269–10280, https://doi.org/10.1021/j100142a004.
[26] E. Vanquelef, S. Simon, G. Marquant, E. Garcia, G. Klimerak, J.C. Delepine, P. Cieplak, F.-Y. Dupradeau, R.E.D. server: a web service for deriving RESP and ESP charges and building force field libraries for new molecules and molecular fragments, Nucleic Acids Res. 39 (Suppl) (2011) W511–W517, https://doi.org/10.1093/nar/gkr288.
[27] R.W. Hockney, J.W. Eastwood, Computer Simulation Using Particles, A. Hilger, Bristol [England]; Philadelphia, 1988 (Special student Ed.).
[28] M. Skowronek, Roterman, L. Konieczny, B. Stopa, J. Rybarska, B. Piekarska, A. Górecki, M. Król, The conformational characteristics of Congo red, Evans blue and Trypan blue, Comput. Chem. 24 (3–4) (2000) 429–450.
[29] H.J.C. Berendsen, D. van der Spoel, R. van Drunen, GROMACS: a message-passing parallel molecular dynamics implementation, Comput. Phys. Commun. 91 (1–3) (1995) 43–56, https://doi.org/10.1016/0010-4655(95)00042-E.

[30] A. Jagusiak, B. Piekarska, T. Pańczyk, M. Jemioła-Rzemińska, E. Bielańska, B. Stopa, G. Zemanek, J. Rybarska, I. Roterman, L. Konieczny, Dispersion of single-wall carbon nanotubes with supramolecular Congo red – properties of the complexes and mechanism of the interaction, Beilstein J. Nanotechnol. 8 (2017) 636–648, https://doi.org/10.3762/bjnano.8.68.

[31] A. Jagusiak, B. Piekarska, K. Chłopaś, E. Bielańska, T. Pańczyk, Shortening and dispersion of single-walled carbon nanotubes upon interaction with mixed supramolecular compounds, Bio-Algorithms Med-Syst. 12 (3) (2016)https://doi.org/10.1515/bams-2016-0015.

[32] S. Woodcock, B. Henrissat, J. Sugiyama, Docking of Congo red to the surface of crystalline cellulose using molecular mechanics, Biopolymers 36 (2) (1995) 201–210, https://doi.org/10.1002/bip.360360208.

[33] A. Di Crescenzo, V. Ettorre, A. Fontana, Non-covalent and reversible functionalization of carbon nanotubes, Beilstein J. Nanotechnol. 5 (2014) 1675–1690, https://doi.org/10.3762/bjnano.5.178.

[34] G. Fiorin, M.L. Klein, J. Hénin, Using collective variables to drive molecular dynamics simulations, Mol. Phys. 111 (22—23) (2013) 3345–3362, https://doi.org/10.1080/00268976.2013.813594.